THE UNIVERSITY OF MICHIGAN

INDUSTRY PROGRAM OF THE COLLEGE OF ENGINEERING

THE EFFECT OF GAMMA PRIME PARTICLE SIZE UPON THE HIGH TEMPERATURE PROPERTIES OF NICKEL-BASE ALLOYS

David L. Sponseller
R. A. Flinn

September, 1960

IP-467

ACKNOWLEDGEMENTS

The authors wish to express their grateful appreciation to all those who have aided in this investigation, and particularly to the following:

The Office of Naval Research, Contract NR-039-065 for financial support during the major part of this investigation.

Dr. J. W. Freeman, Dr. C. M. Hammond, Dr. R. F. Decker, Mr. J. P. Rowe, Mr. R. Jackowski, Mr. E. A. Merriman and Mr. G. N. Maniar for their helpful discussion and assistance.

The Research Laboratory of the International Nickel Company, Inc., for chemical analysis of samples.

The Industry Program of the College of Engineering, University of Michigan, for reproduction of this report.

TABLE OF CONTENTS

	Page
ACKNOWLEDGEMENTS	ii
LIST OF FIGURES	iv
LIST OF TABLES	vi
INTRODUCTION	1
EXPERIMENTAL PROCEDURE	3
I. Ingot Preparation	3
II. Thermal Treatments	4
III. Hardness Measurements	4
IV. Electron Microscopy	5
V. X-Ray Studies	5
VI. High Temperature Testing	6
RESULTS AND DISCUSSION	7
I. Characteristics of γ' Precipitation	7
A. Effect of Composition	7
B. Influence of Precipitating Conditions Upon the Characteristics of γ' Precipitate	12
II. Effect of Dispersion Characteristics Upon High Temperature Properties	23
A. Effects of Relative Amount of γ'	23
B. Effect of Particle Size Upon Creep Properties	25
III. Coherency-Stress Study	33
A. Phase Equilibria	33
B. Lattice Parameter Measurements	34
CONCLUSIONS	38
REFERENCES	39

LIST OF FIGURES

Figure		Page
1	Quasi binary diagram in the Ni-Cr-Al system at 75 At.Pct. nickel	8
2	Electron micrographs of composition series in Ni-Cr-Al system, 16,000 magnification. Specimens aged one hour at 1000°C, furnace-cooled to 750°C, aged 24 hours, air-cooled	10
3	Variation of hardness with composition in aged Ni-Cr-Al specimens	13
4	Electron micrographs of selected aging-time series specimens from heat 451 at 16,000 magnification. Specimens were solution-treated and water quenched prior to aging	15
5	Variation of hardness with aging-time for heat 451	16
6	Effect of cooling rate upon hardness vs composition curves for Ni-Cr-Al specimens	19
7	Effect of the extent of precipitating conditions upon hardness vs composition curves for Ni-Cr-Al specimens	19
8	Effect of aging temperature upon hardness vs composition curves for Ni-Cr-Al specimens	21
9	Exhaustion effect in Ni-Cr-Al system, illustrated by plotting the increment of hardness due to aging the 750°C-aged-specimens at 650°C	21
10	Extremes of as-aged particle sizes of creep specimens from heat 461, at 16,000 magnification	26
11	Variation of second stage creep rate with initial particle size	27
12	Agreement of creep data with the form of Weertman's first and second equations, showing theoretical basis for experimental minimum	30
13	Phase equilibria in the Ni-Cr-Al-Mn system, showing effect of Mn upon extending the γ field	35

Figure Page

14 Expansion of matrix lattice parameter of a Ni-Cr-Al alloy by the separate additions of titanium and manganese 37

LIST OF TABLES

Table		Page
I	CHEMICAL COMPOSITION OF EXPERIMENTAL HEATS	40
II	PURITY OF RAW MATERIALS	41
III	HARDNESS VALUES (VHN)	42
IV	RESULTS OF SHORT-TIME TENSILE TESTS (750°C)	42
V	RESULTS OF CREEP RUPTURE TESTS AT 750°C (1382°F) and 22,500 PSI	43

INTRODUCTION

The control of the amount and size of precipitation-hardening particles in alloys is one of the metallurgist's most powerful methods for improving creep strength at elevated temperatures. It has been used to great advantage in nearly every common alloy system, including nickel-base and cobalt-base alloys, and the precipitation-hardening stainless steels.

In spite of the tremendous importance of the precipitation hardening effect, however, only scant information is available concerning the dependence of high temperature strength and creep rate upon the characteristics of the precipitated dispersion.

Weertman has conducted a theoretical analysis on the relationship between creep strength and the spatial characteristics of a dispersed second phase [1]. Basing his analysis upon the assumption that the rate-controlling process is the climb of dislocations over second-phase particles, he derived three expressions for creep rate. For a given dispersion, the expression that applies depends on the stress level. Each of the three expressions predicts a rather strong dependence of creep strength upon particle size and the mean free path between particles.

It was the purpose of this investigation to study experimentally the influence of the γ' characteristics upon high temperature strength in nickel-base alloys. Specifically, the effects of particle size and of the relative amount of the γ' dispersion were investigated. In addition, the influence of various elements upon coherency effects was explored.

This study was based upon the nickel-chromium-aluminum system at 75 At. Pct. nickel. This rather simple alloy system was chosen in preference to the highly complex commercial nickel-base alloys, so that the dispersion characteristics could be more readily controlled. Phase relationships in this system were studied by Taylor and Floyd[2]. The 750°C (1382°F) reference temperature used by these investigators was chosen as the reference and testing temperature employed throughout this research.

EXPERIMENTAL PROCECURE

I. Ingot Preparation

Thirteen heats of the final analyses shown in Table I were prepared. Four of these, heats 450 through 453, were used for the coherency stress study, while the remaining nine heats, 454 through 462 were for the study of γ' dispersion characteristics.

Heats weighing 3600 grams were melted in a vacuum induction furnace, with the exception of heats 450 through 453 for the coherency investigation. The vacuum melts were conducted in alumina crucibles, while stabilized zirconia crucibles were employed for the air-melted heats. The high purity raw materials are described in Table II.

Cylindrical ingots 2-3/8 inches in diameter by 5-1/2 inches in length were prepared by pouring into molds of heavy-walled steel pipe fitted with an insulating brick hot top and wired to a heavy copper mold stool.

Ingots were homogenized six hours at 1200°C (2192°F) and furnace cooled. They were then hot rolled (1177°C)(2150°F) in increments of three to seven percent per pass using ten-minute reheats. Ingots were rolled down to bars approximately one inch square, representing a reduction in area of 82 percent. After the final pass, all bars were air cooled with the exception of those from heats 459 through 462, which were quenched in oil. The presence of small amounts of boron in all heats permitted the hot rolling to be carried out successfully. There was a significant amount of edge cracking only in heat 458, which contained the highest concentration of aluminum, 14.3

atomic percent. Heat 462, 12.3 atomic percent aluminum, developed minor edge cracks, and the remaining eleven heats, all with lesser amounts of aluminum, were free of edge cracks and any rolling defects.

II. Thermal Treatments

Hot rolled bar stock was subjected to a variety of thermal treatments during the study of the characteristics of γ' precipitation. Thermal treatments are listed in Table III of hardness values. For every speciman a solution treatment preceded the aging treatment. In some cases, a separate solution-anneal-and-water-quench was given the rolled material. Another method of putting the material in the solution-annealed condition involved oil quenching the bars at the completion of hot rolling. In a third method, specimens were solution-annealed immediately prior to cooling to the 750°C (1382°F) aging temperature.

Most of the aging treatments were carried out in conjunction with the third method of solution annealing. This involved furnace cooling or slow step cooling from above the solvus temperature to 750°C, followed by an aging period of at least 24 hours at this temperature.

III. Hardness Measurements

Hardness measurements, listed in Table III, were made at every stage of the processing of the dispersion heats, as well as for several conditions of the coherency heats. For uniformity, surfaces were ground to a roughness approximating No. 100 polishing paper, since it was impractical to polish the large ingots and bars.

in the early stages of processing. Five Rockwell B or Rockwell C readings were taken on every specimen, and the average was converted to a Vickers hardness number (VHN) using the ASTM conversion table A93-52 for nickel-base alloys.

IV. Electron Microscopy

Specimens for electron microscopy were given a final polishing treatment of four hours on a Syntron polishing unit, and then were etched electrolytically with an etchant of the following composition: 56 parts sulfuric acid, 48 parts nitric acid, 14 parts phosphoric acid. Collodion (or alternately pardodion) replicas were then obtained from the specimens. Polystrene latex spheres were then placed on the replicas to provide an internal standard for magnification, and to indicate the direction of shadowing. The replicas were shadowed with palladium to provide contrast.

Phases with shadows in the same direction as the fiducial spheres indicate a depression on the original metal surface. Conversely, phases with shadows opposite to those cast by the spheres are protrusions above the metal surface. An RCA Model EML electron microscope was used to examine and photograph the replicas.

V. X-Ray Studies

Precision lattice constant measurements were made on coherency stress samples, as well as dispersion heat 454. Powder samples were prepared by filing and screening to minus 200 mesh. Samples were annealed in evacuated fused silica tubes for two hours at 750°C (1382°F). X-ray

patterns were made in a North American Phillips symmetrical focusing camera of 12 cm. diameter, using filtered copper radiation. Diffraction lines were analyzed by Cohen's least-squares method.

Preliminary work was done to measure diffraction line widths in the coherency stress phase of this research. This technique was considered as a means of measuring coherency stresses by means of line breaking effects. However, there was insufficient time to carry this work to completion.

VI. High Temperature Testing

Short-time-tensile tests and creep-rupture tests were run on 0.250 inch diameter specimens at 750°C (1382°F). Specimens were held at temperature for four hours prior to the start of either test. Elongations were measured by an optical lever system. The rotating mirrors in the lever system were actuated by hangers suspended from collars on the specimens.

RESULTS AND DISCUSSION

I. Characteristics of γ' Precipitation

In order to conduct a controlled study of the effect of γ' characteristics upon the high-temperature properties of nickel-base alloys, an extensive preliminary program of thermal treatment was carried out. This was done to establish the conditions necessary for producing certain amounts of γ' of the desired particle sizes at 750°C (1382°F). In this phase of the research, the effects of composition and controlled precipitation were investigated, and are considered here.

A. Effect of Composition

Nine heats were prepared in studying the effects of composition upon microstructure and properties of nickel-base alloys. This study was based on the ternary nickel-chromium-aluminum system. In this section, the variation in relative amount of γ' with composition is considered.

1. Phase equilibria

The phase diagram relationships of importance in this study of the nickel-chromium-aluminum system are shown in Figure 1. Here the solvus curves determined by Taylor and Floyd and by Hammond are shown in the quasi binary at 75 atomic percent nickel[2,3]. At the same time, the boundary of the γ' field, based on the work data of Taylor and Floyd is indicated[2]. As is shown by the diagram, the γ' phase, which is an

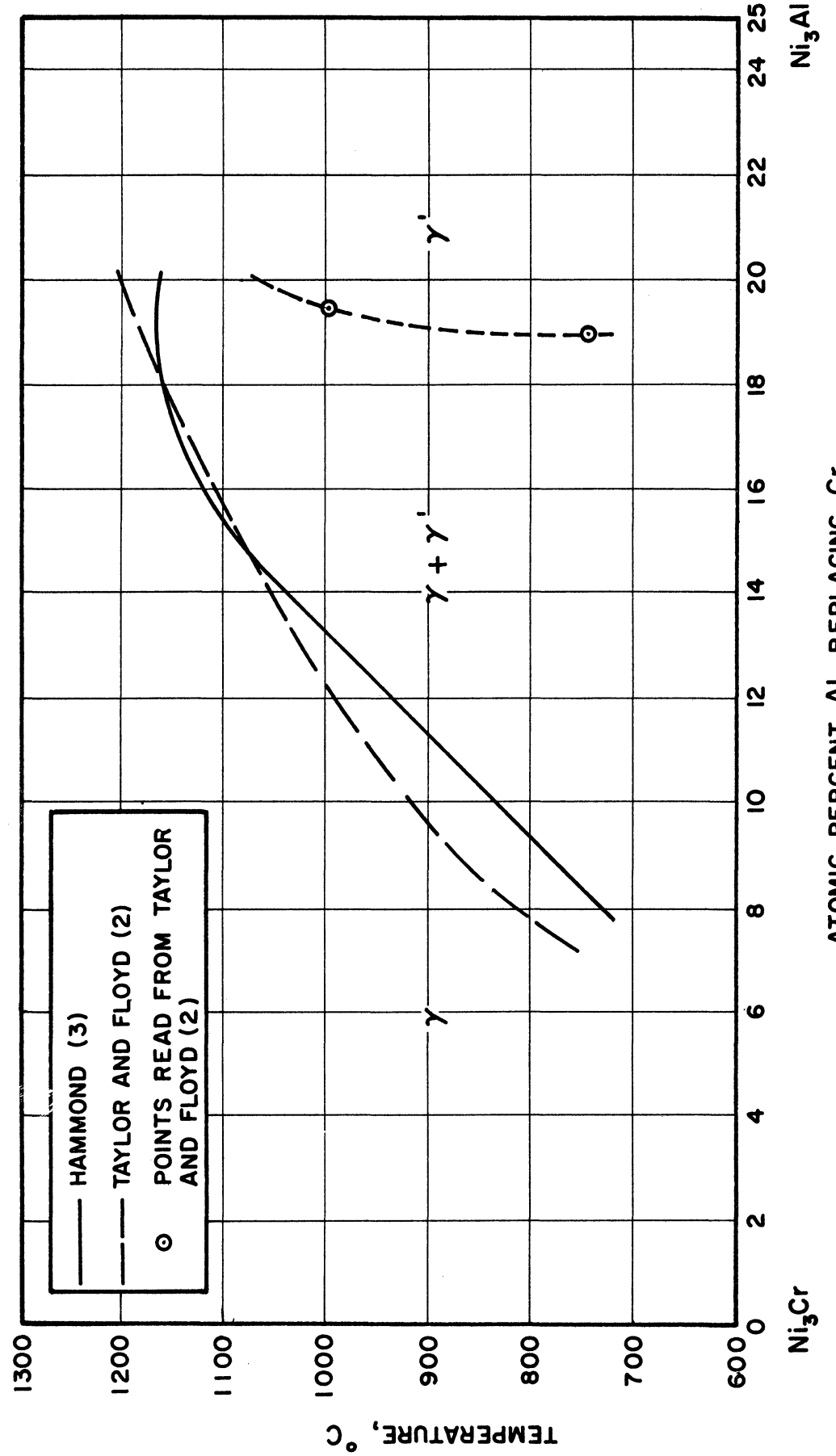

Figure 1. Quasi Binary Diagram in the Ni-Cr-Al System at 75 At. Pct. Nickel

ordered face-centered-cubic structure based on the formula Ni_3Al, is capable of dissolving significant amounts of chromium. However, its composition in equilibrium with the γ matrix phase changes much less with temperature than does that of the γ phase itself. Actually, the lines of the diagram cannot represent equilibrium phase composition since one degree of freedom remains at any temperature when two phases are present in this three-component system. Hence, in the general case the composition of the two phases might be expected to change continuously as alloy composition moves across the two-phase field of the quasi-binary diagram. However, the work of Taylor and Floyd indicates that at the temperature of interest, 750°C (1382°F), the quasi binary lies vitually on a tie line in the ternary isothermal section[2]. Therefore the range of phase compositions encountered at 750°C should be negligible.

2. Relative amount of γ'

Two separate series of heats were prepared to produce various amounts of γ' at 750°C (1382°F). The first series comprised heats 454 (6.39 At. Pct. Al) through 458 (14.3 At. Pct. Al), while the second series consisted of heats 459 (6.25 At. Pct. Al) through 462 (12.3 At. Pct. Al). (The second series was prepared with increased boron content to improve ductility during hot rolling and during high temperature testing.)

Electron micrographs of the first series, as solution-treated at 1000°C (1832°F), furnace-cooled to 750°C (1382°F), held for 24 hours and air-cooled, are shown in Figure 2. Here two main effects may be

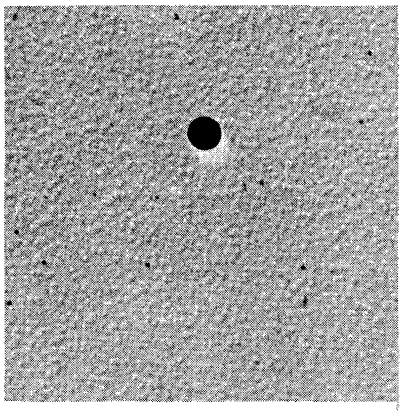

a) Heat 454 (6.39 At. Pct. Al)

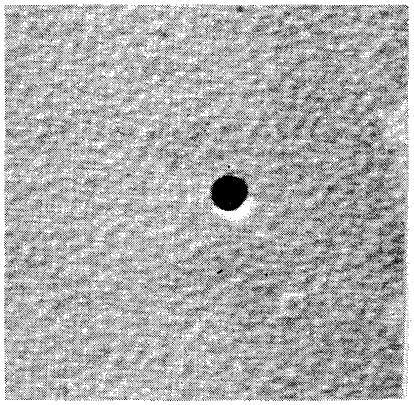

b) Heat 455 (7.27 At. Pct. Al)

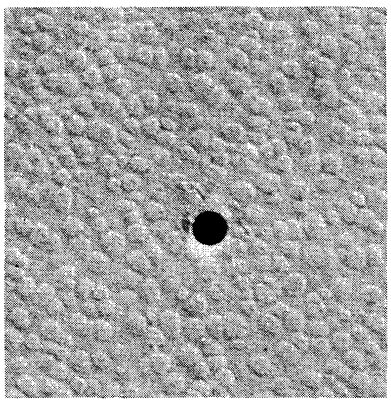

c) Heat 456 (8.26 At. Pct. Al)

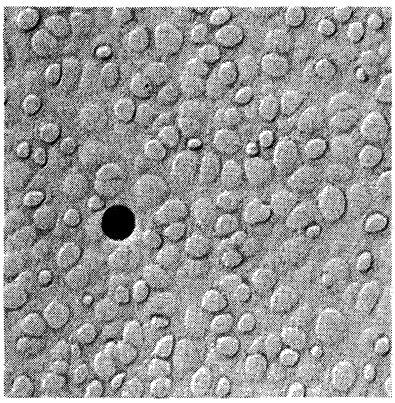

Heat 457 (8.94 At. Pct. Al)

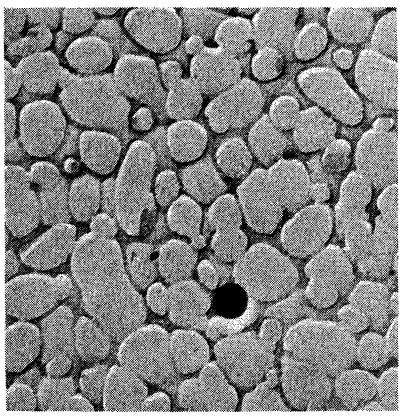

e) Heat 458 (14.3 At. Pct. Al)

Figure 2. Electron Micrographs of Composition Series in Ni-Cr-Al System, 16,000 Magnification. Specimens Aged 1 Hr. at 1000°C, Furnace-Cooled to 750°C, Aged 24 Hr., Air-Cooled

observed. The first effect is that the relative amount of the γ' phase increases quite significantly as the aluminum content increases (and chromium content decreases). In fact, the increase is felt to be much more striking than the micrographs indicate. However, an etching phenomenon presumably causes the lower-aluminum specimens to exhibit much more γ' than they actually contain. This happens because the etchant actually "etches down" to uncover particles that were not exposed on the polished surface before etching. This effect is evident in the 8.94 atomic percent aluminum heat of Figure 2d, where some particles stand out in high relief, while others show very low relief. Because of the etching phenomenon, the volume percent of γ' could not be accurately measured. Any such values in this report are heated at "apparent" volume percent. Also, the nevertheless significant amount of γ' contained in the 6.39 atomic percent aluminum heat of Figure 2a specimen indicates that it very definitely lies in the two phase field of the quasi-binary of Figure 1 and that the solvus curves at the temperature should be displaced considerably to the left at 750°C (1382°F).

3. Particle size

It may be seen from Figure 2 that particle size increases very significantly with increasing aluminum content. The principal reason for this is that the higher aluminum heats cross the solvus line at a higher temperature upon cooling from the solution temperature, thus giving rise to higher diffusion rates and larger particles.

In addition, of course, the larger equilibrium amount of γ' at higher aluminum levels contributes somewhat to the larger particle size.

4. Hardness

Values of hardness for the composition series discussed above are given below, and represented graphically in Figure 3.

Heat No.	454	455	456	457	458
Percent Al	6.39	7.27	8.26	8.94	14.3
Vickers Hardness No.	168	193	222	229	223

These data show that hardness increases quite rapidly initially as the amount of γ' increases. However, a maximum is indicated in the curve, and hardness actually declines at very high aluminum contents. This falling off of hardness presumably results from the very large precipitate size at this level, which causes an overaged condition.

B. Influence of Precipitating Conditions Upon the Characteristics of γ' Precipitate

1. Aging time series

In developing a particle size series in a precipitation-hardening alloy, the method that immediately suggests itself is to employ a series of different aging times. This was done with one of the first heats prepared in this investigation, heat 451. Solution-treated specimens were aged at 750°C (1382°F) for periods ranging from one hour to 1000 hours. The progress of aging was followed with hardness measurements and with electron microscopy of selected specimens.

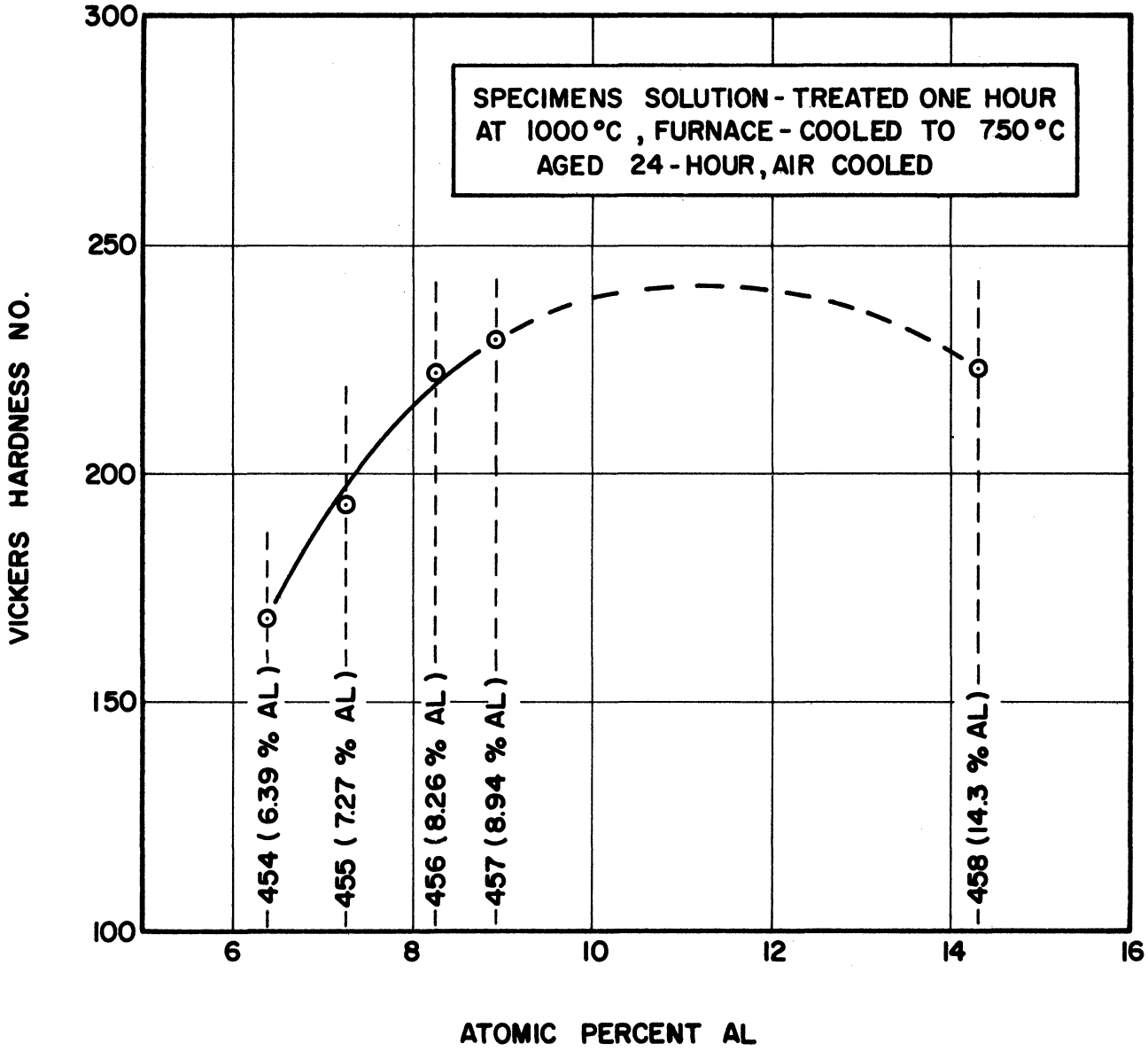

Figure 3. Variation of Hardness with Composition in Aged Ni-Cr-Al Specimens

Hardness values and approximate particle sizes are listed below, with microstructures pictured in Figure 4, and the hardness changes shown graphically in Figure 5.

Aging time (Hr.)	1	4	8	12	24	100	1000
Vickers Hardness No.	334	347	353	357	362	383	332
Approximate particle size (Å)	-	-	175	-	250	-	675

Here the hardness rises quite significantly initially as γ' precipitation occurs. Peak hardness on the curve corresponds to an aging time of 300 hours at 750°C. The estimated particle size at this point is approximately 500 angstroms. The growth of precipitate particles is not very rapid. Even after 1000 hours, the particles seen in Figure 4c are relatively small, 675 angstroms.

Hardnesses in this analysis are at a higher level than those for the other heats in this phase of the investigation, due to the presence of titanium.

2. Nucleation theory

In this investigation, it was desired to determine the high-temperature properties of specimens over a wide range of precipitate sizes, ranging from a few hundred to several thousand angstroms. The results of the aging time series indicated that aging periods of between 5000 and 10,000 hours would be required to achieve the larger sizes.

For this reason, a different approach was used. It seemed necessary to cause γ' to form under conditions favoring only a small

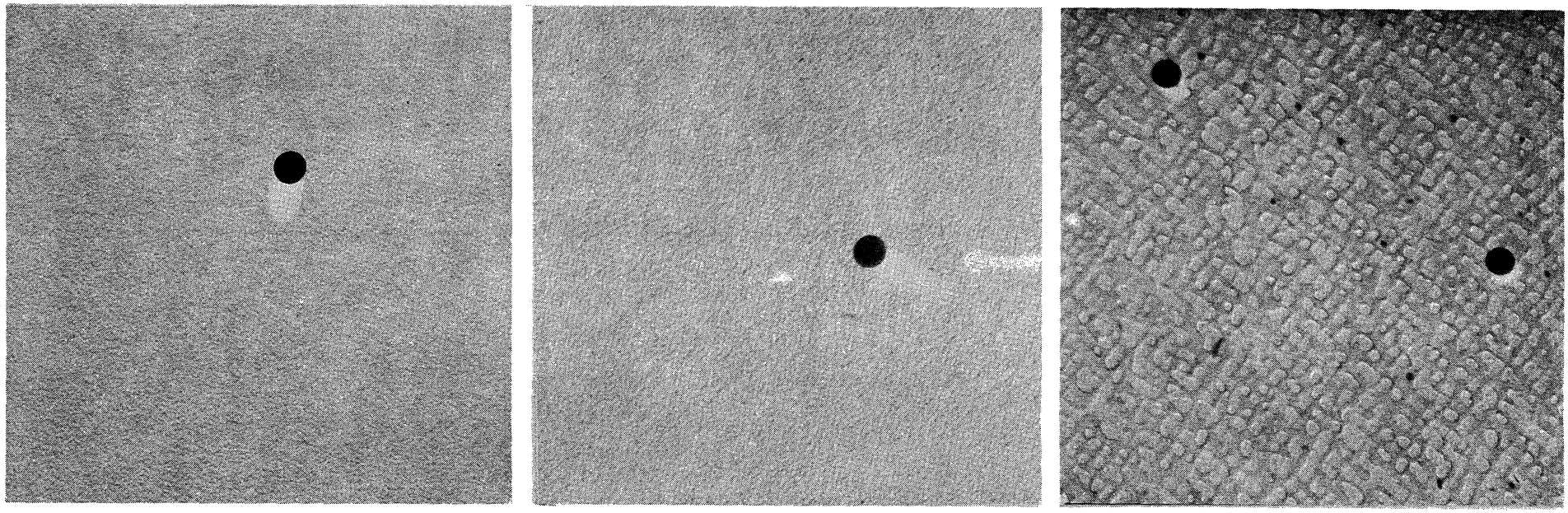

a) Aged 8 Hr., 175 Å Particle Size b) Aged 24 Hr., 250 Å Particle Size c) Aged 1000 Hr., 675 Å Particle Size

Figure 4. Electron Micrographs of Selected Aging-Time Series Specimens from Heat 451 at 16,000 Magnification. Specimens were Solution-Treated and Water Quenched Prior to Aging

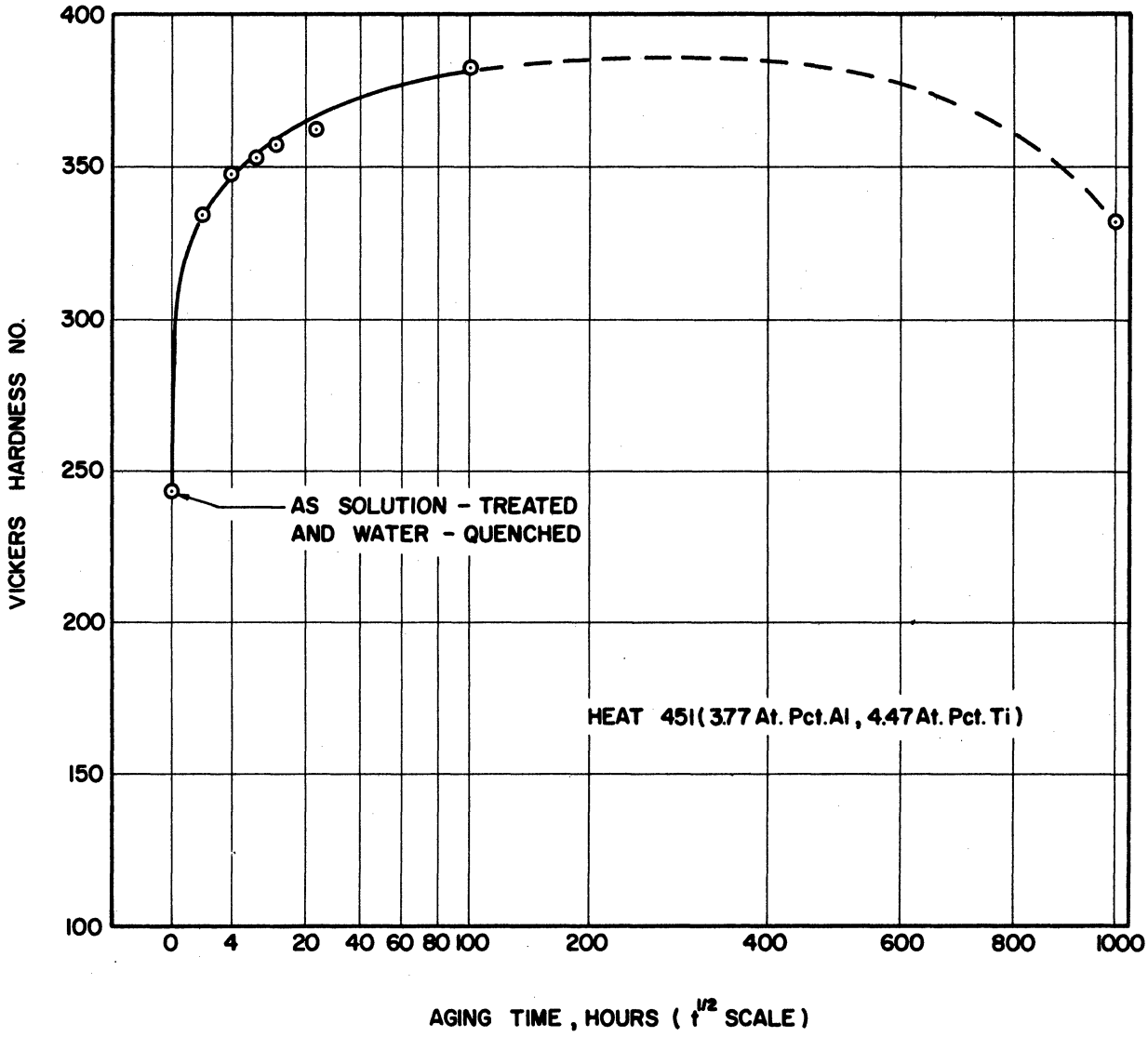

Figure 5. Variation of Hardness with Aging Time for Heat 451

number of nuclei, which in turn could grow to a relatively large size. Nucleation theory suggests a method of accomplishing this. The critical radius, r*, which nuclei of a precipitating phase must attain before they are stable (assuming spherical nuclei and neglecting for simplicity strain energy) is given by the following equation:

$$r^* = \frac{2\sigma}{-\Delta F_V} \text{ cm}$$

where σ = Surface energy, ergs per cm^2

ΔF_V = Bulk free energy change, in ergs per cm^3

Since ΔF_V approaches zero at the solvus temperature, the critical radius approaches infinity. This indicates that it is extremely difficult for stable nuclei to form just slightly below the equilibrium solvus temperature, but that the relative ease of their formation increases as temperature decreases, since r* becomes much smaller.

On this basis, it was decided to cool very slowly from the solution temperature to produce relatively few γ' nuclei and hence large precipitate particles of the phase. This method was in contrast to the classical method of quenching from the solution temperature and then reheating to the aging temperature ... a process that could be expected to yield a very large number of stable nuclei and hence a small particle size. Furthermore, various cooling rates were employed to achieve gradations in particle size. The effectiveness of this method may be observed by comparing Figure 4b with Figure 2c, these figures both representing analyses that should contain approximately 25 atomic percent γ'. Although

both specimens were aged for equal 24-hour periods, the specimen of the latter figure, slowly furnace-cooled from the solution temperature to the aging temperature, contains much larger γ' particles than does the specimen aged by the conventional treatment.

3. Effect of precipitating conditions upon hardness

Several important effects of thermal treatment upon room temperature hardness were observed. An informative comparison can be made between the hardnesses of the original ingots in the as-cast and in the homogenized- and furnace-cooled conditions. These hardness values are plotted in Figure 6, where the slow cooling form of the homogenizing temperature caused superior hardness in the lower aluminum levels, but inferior hardness at the high aluminum level of heat 458, all as compared to the more rapid cooling rate of the casting process. This indicates that hardness is promoted at lower aluminum levels by slow cooling as might be expected, but that beyond approximately nine atomic percent aluminum, overaging is caused by slow cooling.

A more extreme comparison of this type can be made between specimens that were solution treated and water quenched and those that were subsequently very slowly step-cooled from the solution temperature to 750°C (1382°F) and held there for 24 hours. The curves of hardness versus composition for these two conditions are presented in Figure 7.

Considering first of all the solution-annealed and water-quenched condition, virtually no precipitation hardening occurred at the low aluminum levels of heats 454 and 455 during the quench.

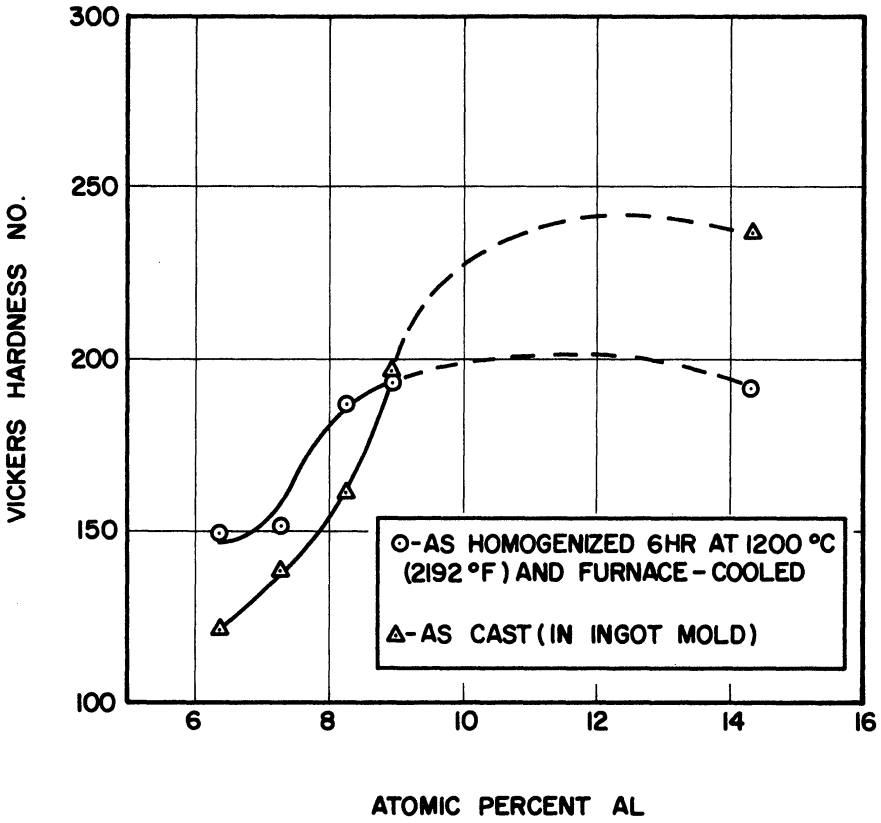

Figure 6. Effect of Cooling Rate Upon Hardness vs. Composition Curves for Ni-Cr-Al Specimens

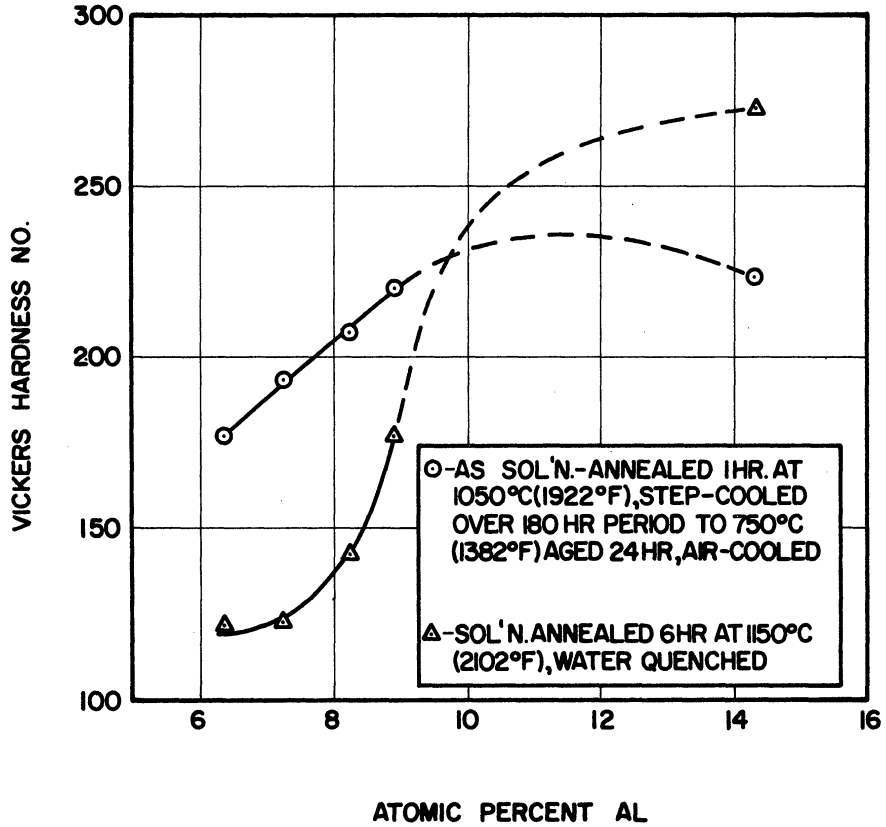

Figure 7. Effect of the Extent of Precipitating Conditions Upon Hardness vs. Composition Curves for Ni-Cr-Al Specimens

However, the high aluminum heat 458 developed the highest hardness of any Ni - Cr - Al specimen observed during this entire investigation, VHN 273. This testifies to the speed of the γ' precipitation at the highest precipitating temperatures associated with high aluminum contents. The other hardness curve of Figure 7 shows that the slow cooling and aging sequence developed much higher hardnesses in the low-aluminum specimens, but caused significant overaging at the high aluminum level of heat 458.

4. Exhaustion effect

The effect of a double aging treatment is shown in the curve of Figure 8. Two series of specimens were step-cooled from the 1000°C (1832°F) solution temperature to the 750°C (1382°F) aging temperature. After 24 hours at this temperature, one set was removed and air cooled, while the other set was step-cooled to 650°C (1202°F) held 24 hours, and air cooled. The hardness curves of Figure 8 show an initial increase of hardness with increasing aluminum contents for both series, followed by overaging in both series in high aluminum heat 458. Part of this overaging is due to the fact that heat 458 is actually below the solvus temperature at 1000°C, as was pointed out in an earlier section. A definite increase in hardness is achieved at all compositions by the second aging treatment. This is due presumably to the larger equilibrium amount of γ' at 650°C (1202°F). The fact that even the "overaged" specimens of heat 458 are hardened slightly by the second aging treatment suggests that precipitation during this stage occurred primarily

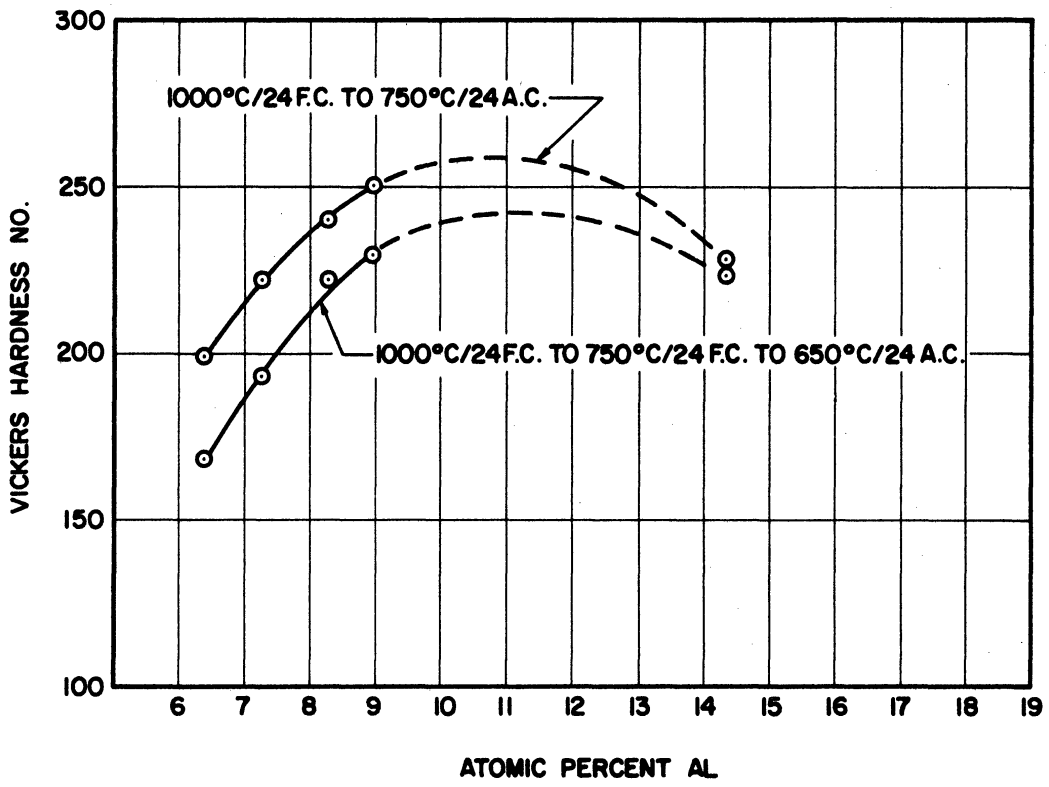

Figure 8. Effect of Aging Temperature Upon Hardness vs. Composition Curves for Ni-Cr-Al Specimens

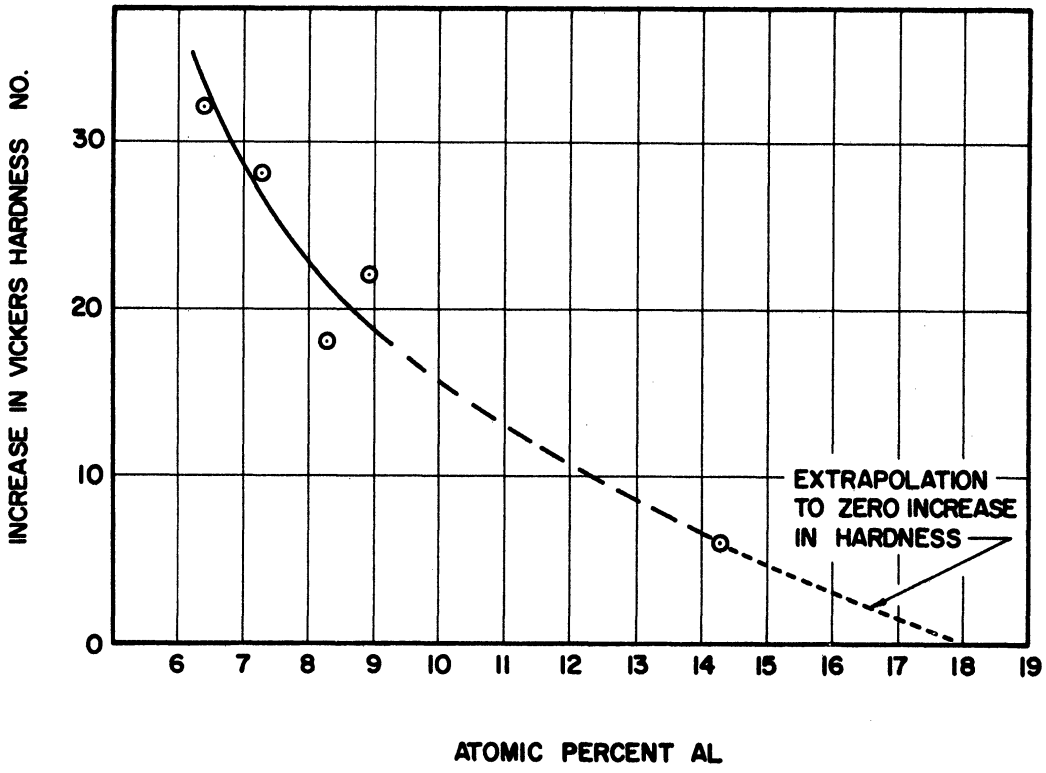

Figure 9. Exhaustion Effect in Ni-Cr-Al System Illustrated by Plotting the Increment of Hardness due to Aging the 750°C-Aged-Specimen at 650°C

in the matrix, rather than on existing particles. Electron microscopy indicates a larger amount of fine matrix precipitate in the 650°C (1202°F) series than in the 750°C (1382°F) series.

An exhaustion effect was observed and is illustrated in Figure 9. Here the increase in hardness due to the second aging treatment is shown. The amount of the increase is seen to diminish as aluminum content increases. The explanation for this is considered to be in the larger amount of the γ matrix phase at lower aluminum levels. The amount of additional γ' precipitation due to the second aging treatment is much lower, therefore, at higher aluminum levels. Hence the higher aluminum heats are relatively "exhausted" in their ability to develop added hardness at lower temperatures, since there is so little matrix phase at such temperatures.

This effect has important implications regarding the temperature dependence of strength properties of alloys of this type, as well as other precipitation hardening alloys, at elevated temperatures. Considering the exhaustion effect in reverse, it is seen that the relative amount of γ' declines much faster with increasing temperature at low aluminum levels than at high aluminum levels. This suggests that in any temperature range, alloys containing small amounts of γ' would be more temperature-sensitive in high temperature strength properties than alloys containing larger amounts of this phase.

An extrapolation of the exhaustion curve to a zero increase in hardness intersects the composition axis at approximately 18 atomic percent aluminum. This bears out the exhaustion effect because this is the approximate boundary of the two-phase field, as seen from Figure 1.

II. Effect of Dispersion Characteristics Upon High Temperature Properties

The underlying purpose of this investigation was to relate the characteristics of the γ' precipitate to the high temperature strength alloys. The results described in the preceding section were used to produce structures having the desired γ' characteristics. Creep tests and short time tensile tests were used to study strength properties at 750°C (1382°F).

A. Effects of Relative Amount of γ'

Tests were run on bars from two heats, aged 24 hours at 750°C (1382°F), to observe the effect of the relative amount of γ' upon high temperature properties. The heats tested contained 6.39 atomic percent aluminum (heat 454) and 8.94 atomic percent aluminum (heat 457). These compositions represent equilibrium volume percentages of 6.6 and 24.7 percent respectively at the aging and testing temperature of 750°C (1382°F), as calculated assuming boundaries in the two-phase field in Figure 1 of 5.5 and 19 atomic percent aluminum, respectively.

1. Short-time-tensile-tests

The results of the high-temperature tests on their heats are listed in Table IV. The short-time-tensile-tests show that a considerably higher yield strength and tensile strength result from

the larger amount of γ' in heat 457. A much smaller elongation accompanies the higher level of strength. The microstructures for these test bars after the aging treatment are shown in Figure 2a and Figure 2d. Here the precipitate particles of specimen 457-3 are seen to be approximately four times greater in diameter than those of heat 454-3. (The volume percentages indicated by these electron micrographs do not lend themselves to an accurate comparison of the true volume percentages, by reason of the etching phenomenon discussed earlier.) While the size difference undoubtedly has some effect in addition to the relative-amount factor, this latter factor is considered to be mainly responsible for the difference in properties between the test bars, for reasons to be discussed in the following section.

2. Creep tests

Creep tests at 750°C (1382°F) and 20,000 psi were performed on similarly aged bars from the same two heats. These tests were not fully satisfactory because the bars ruptured very early in second stage creep before the creep rates could be well established. However, the low-aluminum bar 454-3B deformed at a much higher rate during first stage creep than the high aluminum bar 457-3B. At the time of the last readings, 45 hours, the former had elongated .348 percent, while the latter had elongated just 0.158 percent. This suggests that the relative amount of γ' has a strong influence upon high temperature creep strength.

The premature failure in these bars was apparently due to the low level of boron. For this reason, a second series of dispersion heats was prepared, of higher boron concentrations, for subsequent tests.

B. Effect of Particle Size Upon Creep Properties

Test bars from heat 461 (9.75 At.Pct.Al) were subjected to a variety of aging treatments in order to develop a wide range of γ' particle sizes. These efforts were quite successful, for the particles ranged in size from 270 angstroms in specimen 461-5 to 2460 angstroms in specimen 461-2, the sizes differing by nearly a factor of ten. The extremes of particle sizes are pictured in Figure 10.

1. Second stage creep rates

Aging treatments and creep rupture test results for the five test bars are given in Table V and the second stage creep rates are plotted as a function of particle size in Figure 11. These results show that creep rate initially decreases to a minimum value and then increases, as particle size increases. The minimum in the curve occurs at a particle size of approximately 1200 angstroms.

These results may be shown to bear out the theoretical analysis of Weertman, which predicts the following creep rates in systems containing dispersed particles:

$$K_1 = \frac{\pi \sigma b^3 D}{4\sqrt{2h^2 kT}}$$

for stresses up to $\frac{1}{2}\ \frac{\mu b}{\lambda}$,

$$K_2 = \frac{\pi \sigma^4 \lambda^2 D}{8\sqrt{2h\mu^3 kT}}$$

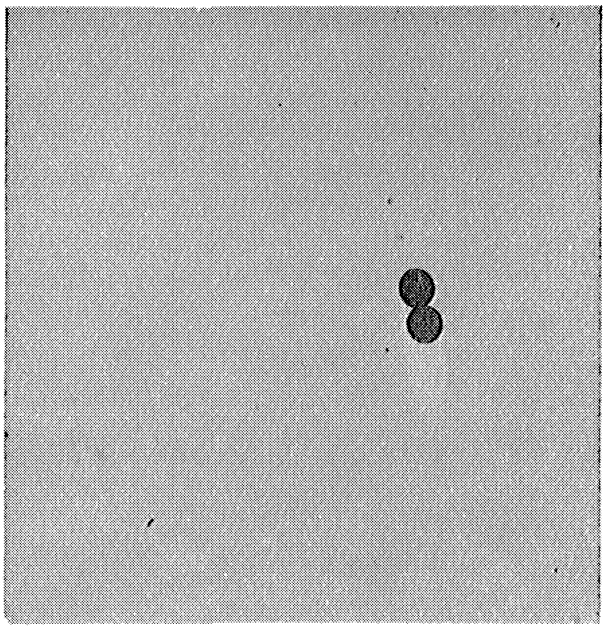

Specimen 461-5. Aged 8 Hr. at 750°C and Air-Cooled.
270 A Particle Size

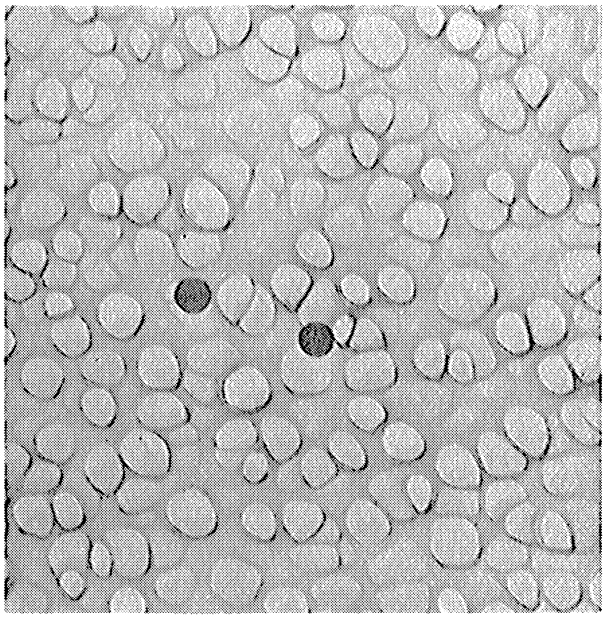

Specimen 461-2. Sol'n Treated 1 Hr. at 1000°C, F.C.
to 750°C, Aged 24 Hr., Air-Cooled.
2450 A Particle Size

Figure 10. Extremes of As-Aged Particle Sizes of Creep Specimens from Heat 461, at 16,000 Magnification

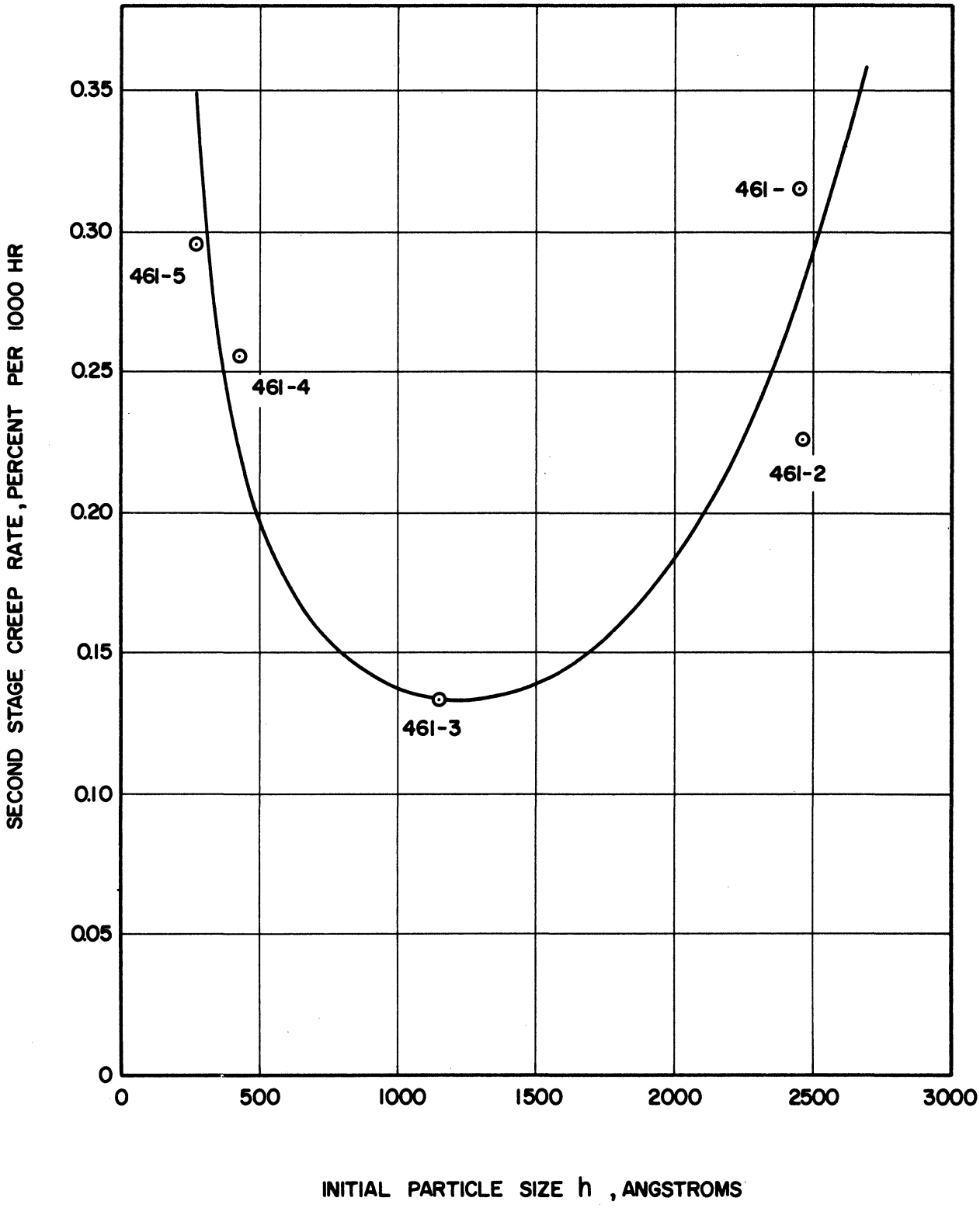

Figure 11. Variation of Second Stage Creep Rate with Initial Particle Size

for stresses up to $(\frac{2\mu kt}{\lambda b^2})^{1/2}$, and

$$K_3 = \left(\frac{\pi\sigma^2\lambda D}{4\sqrt{2}\mu^2 b^2 h}\right) e^{\frac{\sigma^2\lambda b^2}{2\mu kT}},$$

where: K_1, K_2, K_3 = creep rates

σ = stress

b = length of Burgers vector

D = coefficient of self-diffusion

h = particle size

k = Boltzman's constant

T = absolute temperature

μ = $[\frac{1}{2} C_{44} (C_{11} - C_{12})]^{1/2}$ the shear modulus, C_{ij} being the elastic constants.

λ = mean free-path between particles.

While Weertman expresses the dividing lines between the three creep rates in terms of stress, they may also be expressed in terms of the mean free-path, λ. With stress constant at 22,500 psi and the temperature equal to 750°C (1023°K), these values turn out to be:

λ = 404Å, upper limit for K_1

λ = 9350Å, upper limit for K_2

These values were computed using an estimated μ of 5×10^{11} dynes/cm^2, and an interatomic spacing of 2.51Å in the <110> slip direction as the value of b. The values of λ were computed on the assumption that particles of diameter h are distributed in a face-centered-cubic array in the matrix, with the particles occupying the theoretical 31.5 volume percent for the

composition of heat 461. Under these circumstances,

$$\lambda = 0.330h.$$

The above values of λ indicate that the particle sizes encountered in this research would fall within the first two ranges of Weertmen's analysis, and therefore be represented by the creep rates K_1 and K_2. A study of the expressions for these creep rates shows that creep rate should initially decrease as a function of $\frac{1}{h^2}$, and then increase as a function of $\frac{\lambda^2}{h}$ (approximately as a function of .109h for this volume percent). Such a pattern would then predict the minimum in creep rate that appears in Figure 10.

In Figure 12, functions of $\frac{1}{h^2}$ and of h have been fitted to the data points. The particle sizes shown in this figure are the mean values estimated on the basis of a graphical extrapolation to exist during the period of second stage creep. Here, the first two creep rates are accommodated by Weertman's expression for K_1, and the last three by his K_2 expression. The two curves are seem to intersect at λ equals 330 angstroms. This is a remarkable check on Weertman's analysis, which would predict a transition from his first to his second expressions at λ equals 404 angstroms, as noted above.

Further verification of Weertman's analysis lies in the initial values of creep rate for the specimens during first stage creep:

	461-5	461-4	461-3	461-2	461-1
Initial particle size, Å	270	430	1150	2460	2450
Initial creep rate, % per 1000 Hr.	12.5	0.7	1.5	1.4	2.4

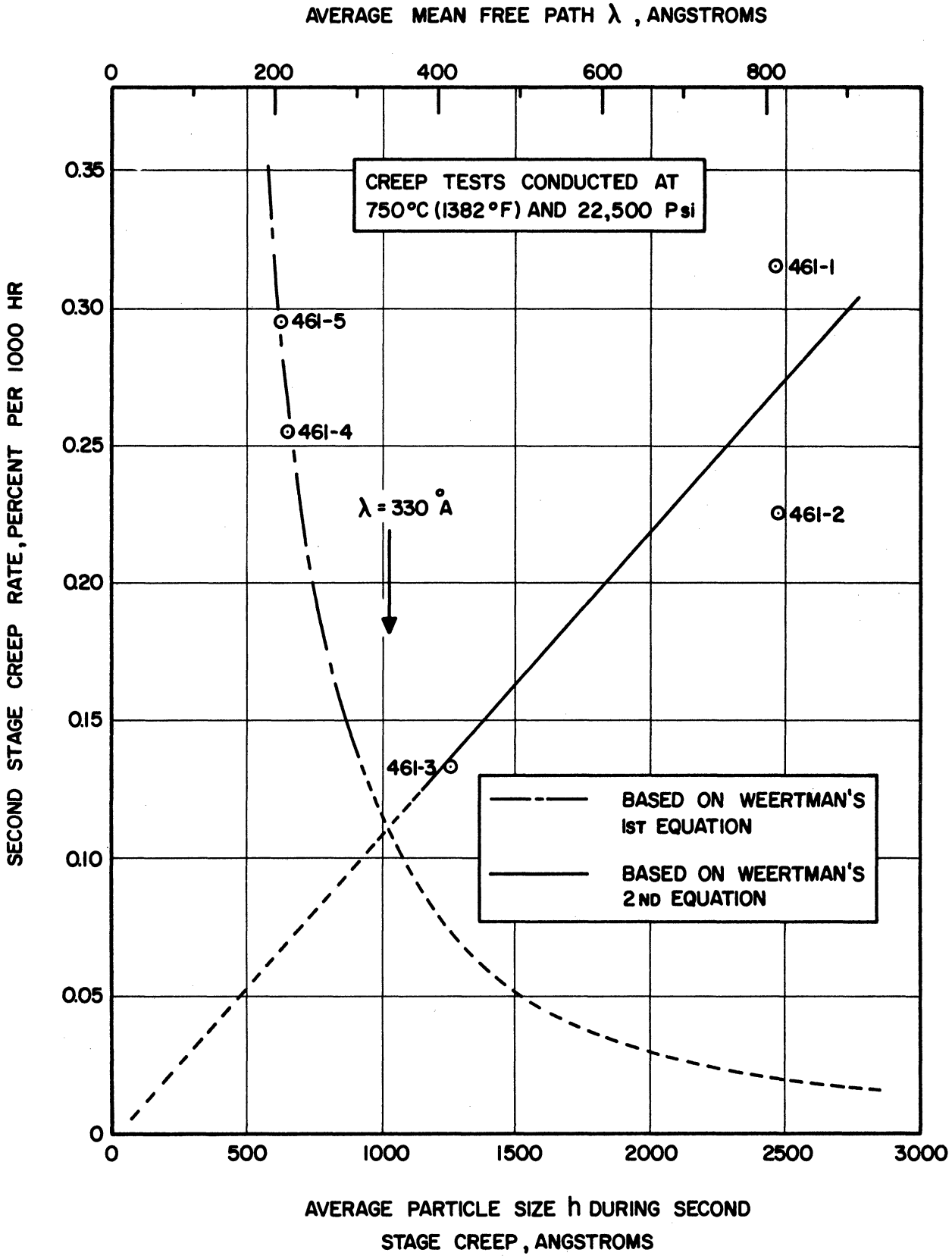

Figure 12. Agreement of Creep Data with the Form of Weertman's First and Second Equations, Showing Theoretical Basis for Experimental Minimum

The much higher rate for specimen 461-5 is attributed to the very small initial particle size resulting from its brief eight-hour aging treatment. This small particle size corresponds to a very high creep rate on the left curve in Figure 12. The other specimens, having larger initial γ' particles at the beginning of the creep tests, presumably did not undergo enough particle coalescence to be shifted so strongly along the curves of Figure 12.

The experimental support for Weertman's analysis observed during this investigation is considered here to have far-reaching implications in the field of high temperature metallurgy. Since creep rate is a minimum at the crossover point from K_1 to K_2, then particle sizes that lie as close as possible to this point should be developed for high temperature engineering components. For particle sizes much less than or greater than the optimum value, inferior creep rate would result.

It would be quite fortuitous if Weertman's analysis should give the precise value of optimum particle size for alloys containing a dispersed second phase. However, the experimental confirmation noted above suggests that Weertman's upper limit for the K_1 expression can be used as an excellent guide, and certainly well within order-of-magnitude accuracy. In terms of mean free path λ,

$$\lambda = \frac{\mu b}{2\sigma}.$$

For nickel-base alloys, assuming values of 5×10^{11} dynes/cm^2 for μ and 2.51 Å for b,

$$\lambda = \frac{9.1(10^6)}{\sigma \text{ (psi)}} \text{ Å} .$$

Here, μ and b do not vary markedly from one alloy system to another, so this expression for optimum-mean-free-path could be used with reasonable accuracy in other systems. (It should be realized that μ varies with temperature, but the exact temperature dependence is not established.)

An important indication from this expression is that creep strength at low stresses if favored by large particle sizes, while fine particle sizes are preferred for high stress applications. The two equations above should serve as an excellent guide in establishing the optimum dispersions for high temperature alloys.

No mention has been made of any coherency effect. It is felt that such an effect could be taken into account by use of an "apparent" particle size h', which would be larger than actual particle size h, to an extent that would depend upon the level of coherency stress.

2. Rupture Lives and elongations

The two creep test bars with the smallest particle sizes have relatively brief rupture lives, as seen from Table V. While one explanation might be the fine particle size, an alternate possibility lies in the method of producing the λ' dispersion. The short-rupture-life bars were aged by the classical method of solution treating, quenching, and aging. However, the three bars that exhibited the long rupture lines were cooled directly from the solution temperature to the 750°C (1382°F) aging temperature, for reasons discussed earlier in this report. Since there is such a striking improvement in rupture life for this group of bars, the special method of aging might very well be responsible.

III. Coherency-Stress Study

A limited amoung of exploratory work was done in this investigation to determine the effectiveness of various elements in promoting high coherency stresses between γ' particles and the matrix of nickel-base alloys. To this end, two heats each were prepared in which titanium and in which manganese were added at two levels of concentration to the basic nickel-chromium-aluminum analysis. It was anticipated that both elements would increase the misfit between the lattices of the matrix and precipitate, thereby promoting higher coherency stresses. The titanium, having a relatively large atomic size, has been found by Taylor to dissolve preferentially in the γ', increasing its lattice parameter (4). Manganese, having a smaller atomic size and being extensively soluble in nickel, was expected to replace chromium in the matrix, reducing the matrix lattice parameter.

A. Phase Equilibria

Electron micrographic studies of specimen's aged at 750°C (1382°F) yielded the following results:

Heat	Composition At. Pct.(Bal. Ni)	Apparent volume percent γ'
450	2.20Ti, 5.44Al, 17.4Cr	30
451	4.47Ti, 3.77Al, 16.4Cr	35
452*	5.00Mn, 10.0Al, 10.0Cr	65
453	9.30Mn, 8.82Al, 4.79Cr	less than 5

* Ann analysis

The two titanium heats were chosen to contain approximately equal amounts of γ' at the 750°C (1382°F) aging temperature, and the data show that this condition was virtually achieved. Since the phase relationships of interest are not known for the Ni-Cr-Al-Mn system, high manganese concentrations were employed to explore the phase equilibria. The data show that the γ' phase is virtually eliminated by going to the higher manganese level. The manganese apparently dissolves extensively in the matrix phase. Figure 13 shows the approximate phase relationships suggested by these data, in which the γ field is quite extensive, presumably extending to the right side of Figure 13 as indicated. This is consistent with the high (35 At. Pct.) solubility of manganese in pure nickel at 750°C.

B. Lattice Parameter Measurements

Precision lattice measurements made on samples aged at 750°C (1382°F) indicate a definite increase in a_o upon the addition of either titanium or manganese to the basic Ni-Cr-Al system. Lattice parameters are as follows:

Heat	a_o, corrected at 25°C (Angstroms)	VHN
454	3.5541	165
450 (2.20 At.Pct.Ti)	3.5583	272
452 (5.0 At. Pct. Mn*)	3.5656	234
453 (9.30 At. Pct. Mn)	3.5759	165

* Aim analysis

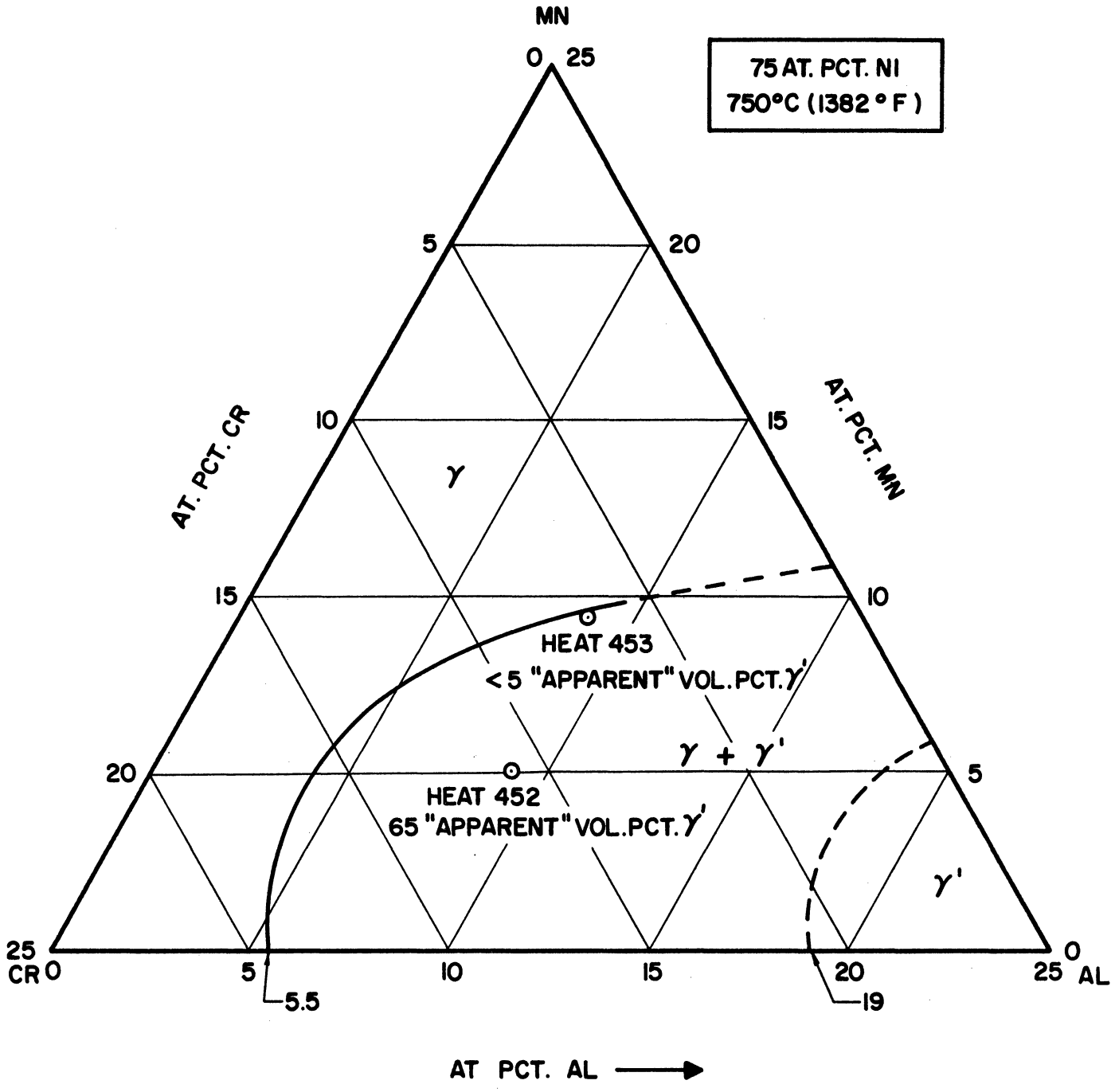

Figure 13. Phase Equilibria in the Ni-Cr-Al-Mn System, Showing Effect of Mn upon Extending the γ Field

These data all refer to samples that were cooled directly to the aging temperature from the solution temperature, and aged for 24 hours. The a_o for heat 454 is included here as a reference value, since this is a Ni-Cr-Al analysis. No separate set of x-ray lines was evident for the γ' phase in any of the x-ray patterns studied, and the above values are considered to be those of the matrix.

The lattice parameters are plotted in Figure 14 where both titanium and manganese are seen to expand the matrix parameter quite significantly. The expansion is linear for the two manganese heats, This expansion by manganese appears at first to be anomalous, since the small atomic size of manganese in its room-temperature allotropic crystal structure would predict the reverse effect. The explanation lies in the fact that the room temperature crystal structure is not face-centered-cubic as is that of the γ matrix phase, but rather complex cubic. The atomic size of manganese in the face-centered-cubic modification is considerably larger, and would, in fact, predict an expansion of the lattice.

The hardness values listed in the above table show that the titanium heat 450 was superior to both the manganese heats 452 and 453. This suggests that the coherency stresses are higher with titanium present than with manganese present, causing a greater hardening effect. The lattice parameter measurements of Taylor show that in the Ni-Cr-Al-Ti system at 1000°C (1832°F) titanium additions expand the γ' lattice much more than the γ lattice, causing the strengthening effect noted above.

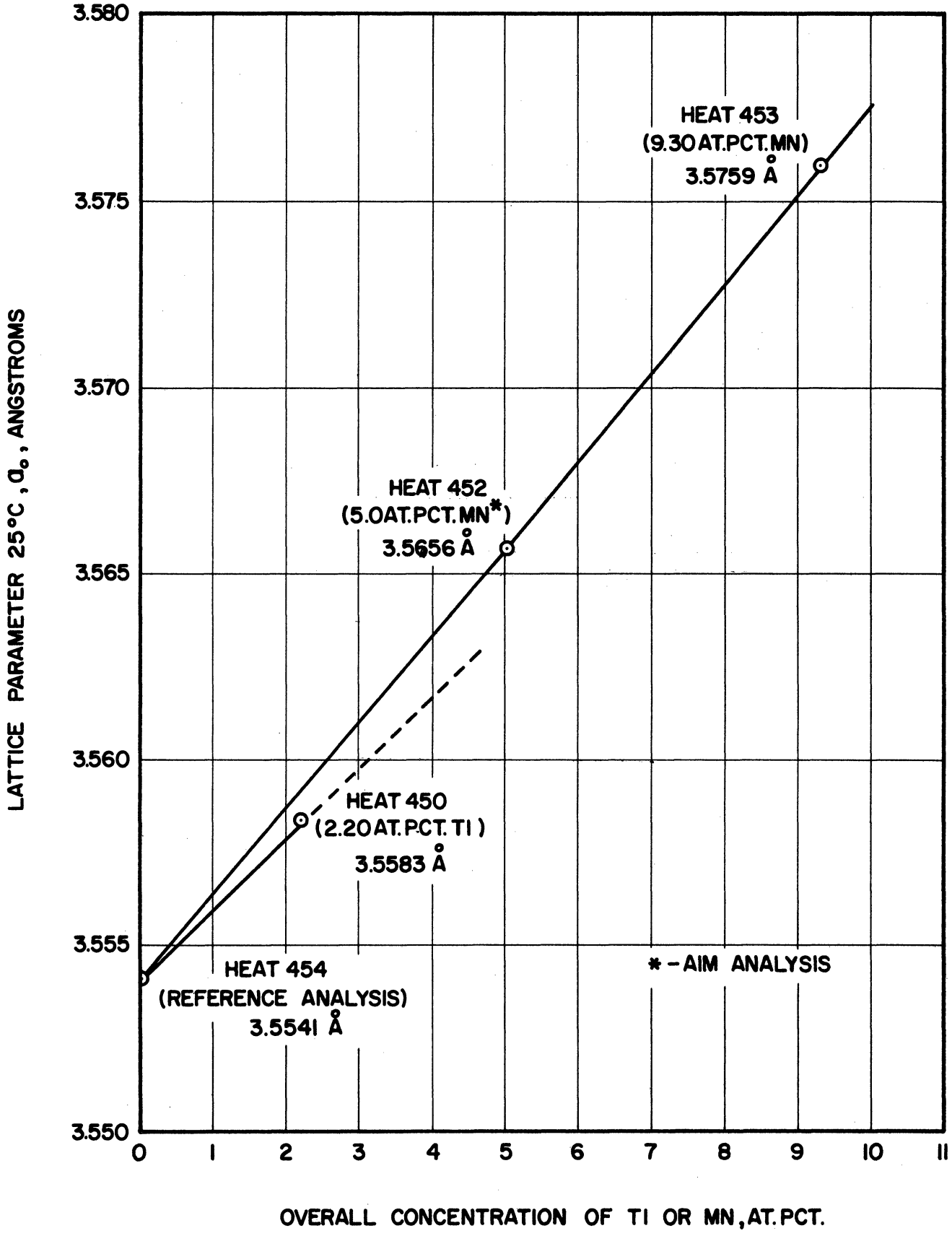

Figure 14. Expansion of Matrix Lattice Parameter of a Ni-Cr-Al Alloy by the Separate Additions of Titanium and Manganese

CONCLUSIONS

The following principal conclusions are made as a result of this investigation, regarding γ'- containing Ni-Cr-Al alloys.

As the aluminum content increases, faster cooling rates from above the solution temperature are required to develop maximum room temperature hardness.

Room temperature hardness, as well as tensile strength and creep strength at elevated temperatures, increase initially with increasing aluminum content.

An exhaustion effect is noted, by which the room temperature hardness of high-aluminum compositions is less sensitive to changes in aging temperature than that of low-aluminum compositions.

Very large particle sizes can be readily developed by slow cooling from above the solution temperature.

An optimum-mean-free-path between γ' particles exists, which results in minimum creep rate. This optimum-mean-free-path (along with the corresponding particle size for a given volume percent of γ') varies with applied stress.

Manganese and titanium expand the lattice of the γ matrix, and manganese reduces the quantity of γ' precipitate.

REFERENCES

1. Weertman, J., "Theory of Creep of Dispersion-Hardened Alloys" Report No. 5123, Naval Research Laboratory, 1958, Washington, D. C.

2. Taylor, A. and R. W. Floyd, J. Institute of Metals, 1952-1953 81, 451.

3. Hammond, C. M., "Ordering and Creep Properties of Ni-Cr-Al Alloys", Doctoral Thesis, University of Michigan, 1959, 39.

4. Taylor, A., J. of Metals, October 1956, 1358.

TABLE I. CHEMICAL COMPOSITION OF EXPERIMENTAL HEATS

Heat No.	Atomic Percent					Weight Percent						
	Ni(1)	Cr	Al	Ti	Mn	Ni(1)	Cr	Al	Ti	Mn	B	C
450	75.0	17.4(2)	5.44(2)	2.20(2)	--	79.2	16.3(2)	2.61(2)	1.92(2)	--	.006(2)	.02(2)
451	75.2	16.4	3.77	4.47	--	78.7	15.6	1.82	3.80	--	.018	.0254
452	75.0	10.0(2)	10.0(2)	--	5.00(2)	80.5	9.51(2)	4.94(2)	--	5.02(2)	.006(2)	.02(2)
453	76.2	4.79	8.82	--	9.30	81.7	9.55	4.93	--	9.30	.006(2)	.01(2)
454	75.4	17.9	6.39	--	--	80.1	16.8	3.12	--	--	.0027	.0070
455	75.2	17.2	7.27	--	--	80.2	16.2	3.57	--	--	.0039	.0160
456	75.1	16.3	8.26	--	--	80.5	15.4	4.07	--	--	.0041	.0082
457	75.6	14.9	8.94	--	--	81.4	14.2	4.42	--	--	.0034	.0116
458	75.3	10.3	14.3	--	--	82.8	10.0	7.21	--	--	.0023	.0080
459	76.1	17.7	6.25	--	--	80.4	16.5	3.04	--	--	.015	.0074
460	74.3	17.6	8.31	--	--	79.2	16.7	4.07	--	--	.018	.0052
461	75.0	15.1	9.75	--	--	80.8	14.4	4.83	--	--	.016	.0042
462	74.5	13.2	12.3	--	--	81.0	12.8	6.17	--	--	.017	.0070

(1) Nickel obtained by difference

(2) Not analyzed. Value based on aim analysis (carbon concentrations estimated for heats 450, 452, and 453.)

TABLE II

PURITY OF RAW MATERIALS

	Percent Impurities						
	C	Fe	Si	O	H	N	S
Electrolytic Ni	trace	<0.04	-----	.003	.0004	.00009	trace
High Purity Electrolytic Cr(99.95%)	0.004	0.003	0.004	.016	.0001	.009	.005
Aluminum (99.99%)	-----	-----	-----	----	-----	------	-----
Manganese (99.9%)*	-----	-----	-----	----	-----	------	-----
Titanium *	.02	.20	-----	.12Max	-----	.02	-----
Nickel-boron (17.3%B)	0.61	2.34	<0.50	.009	.0006	.0002	-----
Shield alloy*	.02	.30	.11	----	----	-----	.026

* Used for heats 450 - 453 only.

TABLE III. HARDNESS VALUES (VHN)

Heat No.	454	455	456	457	458	459	460	461	462
As Cast	121	138	161	197	237	122	183	234	253
Homogenized, F.C.	149	151	187	193	192	153	202	219	251
Hot rolled, A.C.	159	210	242	241	263				
Hot rolled, O.Q.						124	171	200	257
1000° C/1 Step-cooled to 750°C over 180-Hr. period, 750°/24.						144	211	226	242
1000° C/24, Step cooled 25° C/30 min to 750° C, 750°C/24*	168	193	222	229	223				
1000° C/24, Step cooled 25°C/30 min to 750°C, 750°C/24, Step cooled 25°C/30 min to 650°C, 650°C/24	199	221	240	250	228				
Sol'n Anneal; 1150°C/6, W.Q.	122	123	143	177	273				
Sol'n Anneal; 1000°C/1, F.C. to 750°C, 750°C/24	165	181	196	213	248				
Sol'n Anneal; 1050°C/1, Step Cooled to 750°C over 180-Hr. period, 750°C/24	177	193	207	220	223				

* All aged specimens air-cooled from the aging temperature.

TABLE IV RESULTS OF SHORT-TIME TENSILE TESTS (750°C)

Spec. No.	Calculated Wt. % γ'	Aging Treatment	0.2% Y.S.	T.S. (Psi)	Elongation (% in 1 inch)
454-3A	7	1000°C/1, F.C. to 750°C/24, A.C.	39,500	60,000	11
457-3A	25	same	60,300	73,800	3

TABLE V RESULTS OF CREEP RUPTURE TESTS
AT 750°C (1382°F) AND 22,500 PSI

Spec. No.	Aging Treatment	γ' Particle Size After Aging Treatment (Angstroms)	Second Stage Creep Rate (% / 1000 Hr.)	Rupture Life (Hr.)	Elongations (%)
461-5	750°C(1382°F)/8	270	0.295	210	1
461-4	750°C/32	430	0.255	265	1
461-3	1000°C(1382°F)/1, direct transfer to 750°C/48	1150	0.133	1125	1
461-2	1000°C/1, F.C. to 750°C/48	2460	0.225	1031	1
461-1	1000°C/1, F.C. to 875°C (1607°F)/24, F.C. to 750°C/24	2450	0.315	1109	2